CHAPTER EIGHTEEN

Single mRNA Tracking in Live Cells

Hye Yoon Park, Adina R. Buxbaum, *and* Robert H. Singer

Contents

Abstract

Asymmetric distribution of mRNA is a prevalent phenomenon observed in diverse cell types. The posttranscriptional movement and localization of mRNA provides an important mechanism to target certain proteins to specific cytoplasmic regions of their function. Recent technical advances have enabled real-time visualization of single mRNA molecules in living cells. Studies analyzing the motion of individual mRNAs have shed light on the complex RNA transport system. This chapter presents an overview of general approaches for single particle tracking and some methodologies that are used for single mRNA detection.

Anatomy and Structural Biology and Gruss-Lipper Biophotonics Center, Albert Einstein College of Medicine, New York, USA

Methods in Enzymology, Volume 472
ISSN 0076-6879, DOI: 10.1016/S0076-6879(10)72003-6

1. Introduction

Localization of mRNA is an important mechanism to generate cell polarity crucial in diverse cellular functions from motility to differentiation (for reviews, see Condeelis and Singer, 2005; Martin and Ephrussi, 2009; Shav-Tal and Singer, 2005). The asymmetrical distribution of mRNA provides a means for a cell to regulate the protein synthesis at high spatial and temporal resolution. Localized mRNAs can be translated repeatedly to produce high concentrations of proteins in specific subcellular compartments in response to local stimuli. To date, thousands of mRNAs are found to exhibit spatially distinct patterns in many different cell types, including budding yeast, fruit fly oocyte, fibroblasts, and neurons (Martin and Ephrussi, 2009).

Technical developments in intracellular RNA imaging have been indispensable to increase our knowledge about the mechanisms of mRNA localization. When the localization of β-actin mRNA was first observed in the lamellipodia of fibroblasts (Lawrence and Singer, 1986), the mRNAs were hybridized with radioactive DNA probes and visualized by autoradiography, which required exposure times in the range of weeks. Now, it is possible to observe the movement of single mRNA molecules in living cells in real time (Bertrand *et al.*, 1998; Fusco *et al.*, 2003; Shav-Tal *et al.*, 2004).

Single particle tracking (SPT) is used in many different research fields to investigate the dynamics of individual objects by regarding them as punctate points while ignoring the internal conformations. By following the trajectories of particles, we can characterize the types of motion and measure the velocity or diffusion coefficient. Jean Perrin, probably in the first SPT akin to modern methods, observed the movements of gamboges with submicron precision (Perrin, 1913). His quantitative analysis of the trajectories supported Einstein's microscopic theory of Brownian motion (Einstein, 1905). In cell biology, the use of SPT was pioneered by Barak and Webb (1982). They observed the motion of fluorescently labeled low-density lipoprotein (LDL) receptors on plasma membrane. De Brabander *et al.* (1985) microinjected colloidal gold particles of 20–40 nm in living cells, and visualized their motion using transmitted light To date, SPT has been extensively used to study complex cellular dynamics, including ligand–receptor interactions, membrane organization, secretory granules, locomotion of motor proteins, and transport within nuclei (reviewed in Kusumi *et al.*, 2005; Levi and Gratton, 2007; Saxton and Jacobson, 1997; Wieser and Schutz, 2008).

There are other optical techniques for measuring the lateral mobility. In the technique of fluorescence recovery after photobleaching, or FRAP (Axelrod *et al.*, 1976), a region of interest is irreversibly photobleached by

intense laser irradiation and then, recovering fluorescence in the area is recorded in time. From the recovery curve, one can derive the fraction and the diffusion coefficient D of mobile fluorescent molecules. Caution is required, however, in the presence of multiple species with distinct characteristics of mobility: FRAP data are an ensemble average of the total population, and the specific dynamics of a subpopulation may be hidden. SPT overcomes this limitation of FRAP by directly observing individual particles. Furthermore, the spatial resolution of SPT exceeds that of FRAP by more than an order of magnitude. SPT considers only the center of particles which can be determined with a precision of one to tens of nanometers, whereas the diffraction-limited focal volume dictates the minimum area in FRAP or fluorescence correlation spectroscopy (FCS). Consequently, SPT is suitable for high-resolution studies, far below the diffraction limit, of nanometer-scale displacements and structures, such as motor proteins and membrane microdomains.

Here, we describe SPT techniques that have been applied to the studies of mRNA trafficking in living cells. Methods to label, visualize, and track single mRNA molecules are reviewed. The ''MS2 system'' (Beach *et al.*, 1999; Bertrand *et al.*, 1998) for labeling mRNA is emphasized, which has been established in our laboratory. Various analysis techniques are reviewed and the information obtained by combining SPT with the MS2 system is discussed toward the end of the chapter.

2. Significance of Tracking mRNA

Many aspects of mRNA transport and localization have been discovered by single mRNA imaging and tracking. Whereas *in situ* hybridization shows the distribution of mRNA fixed at different stages, tracking of single mRNAs can reveal the *in vivo* dynamics that occur in the native environment. Tracking single mRNA particles in the cytoplasm of COS cells revealed that the movement of a reporter mRNA in the cytoplasm could be diffusive, static, corralled, and directed, with diffusive motion dominating (Fusco *et al.*, 2003). The authors of this study were also able to show for the first time the movement of mRNA along cytoskeletal fibers. Interestingly, the addition of the β-actin 3′UTR to the construct, which contains a localization sequence necessary for the localization of β-actin mRNA, increased in the relative amount of directed movements and their average length. In a related study, single molecule tracking allowed the measurement of the diffusion coefficient of β-actin mRNA in different regions of the COS cells. β-actin mRNA was found to diffuse freely in the leading edge of the cell, however, in the perinuclear region, mRNA diffusion was restricted. Disruption of the actin cytoskeleton delocalized mRNA

and increased the diffusion coefficient of mRNA in the perinuclear region, indicating that cytoskeletal barriers may play a role in the localization of β-actin mRNA (Yamagishi *et al.*, 2009).

In an additional study where SPT was critical to probing a mechanism of mRNA localization, Bertrand *et al.* (1998) employed single mRNA tracking to address the question of how ASH1 mRNA travels to the bud tip in yeast. It was known that SHE1/MYO4, a type V myosin, as well as an intact actin cytoskeleton were necessary for ASH1 mRNA localization, however, it was not clear whether ASH1 mRNA was actively transported to the bud tip or if myosin was transporting another protein necessary for ASH1 mRNA anchoring at the bud tip. Real-time imaging and particle tracking indicated that ASH1 was transported from mother to daughter yeast cell with a velocity consistent with motor-based transport and that mRNA particles colocalized with myosin.

Single mRNA tracking in the nucleus was used to address the controversial question of how mRNA travels in the nucleus, revealing movements indicative of corralled diffusion (Shav-Tal *et al.*, 2004). In this study, it was shown that mRNAs are not actively transported in the nucleus but passively diffuse. Zimyanin *et al.* (2008) also used live cell visualization and tracking of mRNA to address a controversy in the field of *oskar* mRNA localization in *Drosophila* oocytes. Prior to their study, it had been known that kinesin was necessary for posterior *oskar* mRNA localization, so seemingly *oskar* mRNA localization depended on kinesin-based transport; however, paradoxically, the microtubule network in the *Drosophila* oocyte lacks uniform polarity. Other theories postulated that cytoplasmic flow or exclusion from specific regions are responsible for *oskar* mRNA localization, with kinesin playing an indirect role. By direct observation of the mRNA, the authors showed that the mRNA moves along microtubules in many directions with a 14% bias toward the posterior region. Over time, this is sufficient to localize the mRNA to the correct region in the appropriate time frame.

An interesting cellular model for active transport of mRNA is the study of mRNA localization in neuronal processes, as diffusion alone is insufficient to transport mRNA into long dendritic processes, thus, active transport is a necessity for mRNA to reach the distal regions of neurons. Live imaging of calcium/calmodulin kinase II alpha reporter mRNA revealed a kinesin and microtubule-dependent oscillatory movement of the mRNA in the dendrites. Following stimulation, there is an increase of mRNA movement in the anterograde direction, bringing mRNA granules into dendrites and increasing the probability of arriving at activated synapses (Rook *et al.*, 2000). These representative examples emphasize the significant discoveries in the field of mRNA trafficking where live mRNA imaging and tracking played a pivotal role in understanding the mechanisms of mRNA localization.

3. Labeling mRNA in Living Cells

3.1. Selection of probes for SPT

A wide variety of probes have been used in SPT, including gold particles, quantum dots, small organic dyes, and fluorescent proteins. Colloidal gold particles of 20–40 nm in diameter have been used with bright field microscopy (De Brabander *et al.*, 1985) or differential interference contrast (DIC) microscopy (Sheetz *et al.*, 1989). A small number of ligands or Fab fragments of the antibody IgG for target molecules are conjugated to the gold particles. Labeling by gold is advantageous for longer duration of tracking because there is no photobleaching and little saturation. Also, it allows the manipulation of single particles by using an optical trap (Edidin *et al.*, 1991; Kusumi *et al.*, 1998). However, gold probes have artifacts such as nonspecific charge interactions and crosslinking (Kusumi *et al.*, 2005) and have not been yet applied successfully to mRNA labeling in living cells.

Fluorescent probes are more amenable to specific labeling. Simultaneous tracking of different species is readily achieved by multicolor imaging with diverse fluorescent tags. When using fluorescent probes, photostability and brightness are the primary figures of merit for SPT. Quantum dots have been widely used for SPT since they are 10- to 100-times brighter and 100- to 1000-times more photostable than organic dyes (Smith *et al.*, 2008). Another advantage of semiconductor nanocrystals is that the emission wavelength can be tuned by the size; larger quantum dots emit redder fluorescence. However, quantum dots exhibit intermittent emission, or "blinking" (Nirmal *et al.*, 1996), which can complicate the analysis of SPT data. Using quantum dots, Ishihama and Funatsu observed the movement of single mRNAs for over 60 s with a time resolution of 30 ms (Ishihama and Funatsu, 2009).

Organic dyes and fluorescent proteins have been predominantly used for labeling mRNAs (for reviews, see Querido and Chartrand, 2008; Rodriguez *et al.*, 2007; Tyagi, 2009). To image total mRNA in live cells, nonspecific nucleic acid stains such as SYTO 14 can be used (Knowles *et al.*, 1996). Visualization of specific mRNA has been typically achieved through the microinjection of fluorescently labeled RNAs (Ainger *et al.*, 1993; Shan *et al.*, 2003; for a review of fluorescent RNA cytochemistry, see Pederson, 2001). An alternate technique that allows the labeling of endogenous mRNA is a variation of FISH performed on live cells. Santangelo *et al.* (2009) describe a technique where the membranes of live cells are reversibly permeabilized with the Streptolysin O, which delivers fluorescently labeled oligonucleotides into cells. Finally, molecular beacons have also been used to visualize endogenous mRNAs in live cells (Bratu *et al.*, 2003), where delivery also typically involves microinjection.

3.2. The MS2-GFP system

To label native mRNA with GFP in living cells, the MS2-labeling technique has been devised (Bertrand *et al.*, 1998). High autofluorescence in the cytoplasm can significantly confound tracking single molecules in a live cell. In order to enhance the signal-to-background ratio, the system expresses mRNAs that contain multiple MS2 stem loops, to each of which a dimer of fluorescent protein-fused MS2 coat proteins (FP-MCP) specifically binds. We have empirically determined that 24 copies of the MS2 binding sites (MBS) binding up to 48 FP-MCPs are sufficient to visualize single mRNA molecules (Fusco *et al.*, 2003; Shav-Tal *et al.*, 2004). Plasmids containing multiple MBS cassettes and FP-MCP are available upon request at http://singerlab.aecom.yu.edu/requests/.

The benefit of using genetically encoded fluorescent proteins to label mRNAs is that the mRNA is transcribed and labeled in the nucleus, which should ensure proper binding of mRNA binding proteins, necessary for proper export, transport, and translation (Farina and Singer, 2002). Additionally, the MS2 system involves minimal perturbation to the cellular structure as opposed to other methods of delivery of exogenous mRNA such as microinjection of fluorescently labeled mRNAs or delivery through the perturbation of the plasma membrane. Many previous chapters have addressed the methodology using the MS2 system to fluorescently label mRNAs (Chao *et al.*, 2008a; Grunwald *et al.*, 2008b). This chapter will focus on technical considerations as opposed to specific instructions.

An MS2-GFP labeling system should be designed properly with several considerations. It is important that the MS2-GFP construct includes appropriate untranslated regions (UTR), which play an essential role in the mRNA localization by regulating the mRNA's interaction with the cytoskeleton or RNA binding proteins. Moreover, the MS2 repeats must be inserted in a carefully selected location. It is highly recommended to verify proper trafficking of mRNA using FISH in order to avoid potential problems. Other unknown elements not included in the reporter construct may be important for correct localization. Or the MS2 repeats may interfere with trafficking or induce nonsense-mediated degradation of the mRNA.

Secondly, appropriate levels of expression are crucial. If both the reporter mRNA and the FP-MCP are overly expressed, they may form fluorescent aggregates in the cytoplasm of the cell. Overexpression of mRNA may also lead to abnormal localization, because RNA-binding proteins and transport machinery may exist in limiting amounts. Therefore, it is most desirable that the reporter constructs are expressed under their own promoters. Retrovirus or lentivirus infection is widely used for creating stably expressing cells. Because each cell will only contain a few copies of the transgene, this method not only eliminates the concern of overexpression but also reduces the cell-to-cell variations in expression.

When performing live cell imaging using the MS2 system, multiple controls are essential to perform to verify the correct trafficking of the mRNA. MS2-tagged mRNAs should be visualized in combination with FISH to measure the relative abundance of labeled mRNAs, as in Fusco *et al.* (2003). Furthermore, FISH should be performed on cells that express the stem-loop-tagged mRNA in the absence and presence of the FP-MCP to ensure proper targeting of the mRNA with the stem loops and while bound to multiple fluorescent proteins. An additional necessary control is to express the FP-MCP in cells that do not contain the stem-loop-tagged mRNA for the purpose of verifying that the expression of the coat protein does not lead to artifactual aggregation of fluorescent protein in the cells.

In our laboratory, a transgenic mouse line with 24 MS2 repeats inserted into the 3′UTR of the β-actin gene has been created recently (manuscript in preparation). This system will allow the visualization and tracking of endogenous β-actin mRNA in various cell types, and moreover *in vivo*, which has not been achieved before. An orthogonal system for RNA labeling has also been developed using PP7 bacteriophage coat protein (Chao *et al.*, 2008b), which will enable the tracking of multiple mRNA species.

3.3. Minimizing photobleaching and phototoxicity

Ultimately, long time-lapse imaging experiments are limited by photobleaching and phototoxicity. The average number of photons emitted by a dye molecule before photobleaching is approximately 10,000–100,000. Photobleaching occurs by several complex mechanisms and strongly depends on the environmental conditions such as solvent polarity and temperature (Eggeling *et al.*, 2005). The most notable mechanism for photobleaching is photooxidation. Fluorophores in triplet excited state react with ground-state triplet oxygen and generate singlet oxygen ($^1O_2$). The highly reactive singlet oxygen causes both photobleaching and phototoxicity. Several reagents such as ascorbic acid and enzymatic deoxygenation systems have been used to reduce the detrimental effects. However, the removal of oxygen can enhance or reduce the photobleaching effect depending on the experimental condition. This is because photooxidation processes cause both the ground-state recovery of the dyes and the formation of irreversible photoproducts. Therefore, the concentration of oxygen scavengers needs to be optimized for sufficiently long tracking experiments. Addition of triplet quenchers such as Trolox (a water-soluble analog of vitamin E) and mercaptoethylamine can also improve the photostability (Rasnik *et al.*, 2006; Widengren *et al.*, 2007).

4. Imaging mRNA Movements

4.1. Experimental considerations

In order to track single mRNA movement in real time, it is important to achieve high sensitivity for single molecule detection and fast image acquisition. In fluorescence microscopy, photobleaching phenomena inherently limit the number of photons available from the probe. Therefore, one needs to find a good balance in the image-acquisition protocol.

First, the camera exposure time needs to be optimized to detect single molecules in motion. The precision to locate the center of a particle is proportional to the total number of collected photons (Bobroff, 1986). Once the imaging system is optimized for the highest signal-to-noise ratio, the exposure time needs to be long enough to locate particles with a desirable precision. On the other hand, the camera exposure has to be short enough to capture an image of a highly mobile object. If the particle travels a significant distance during the exposure time, it will show up as a streak or a blurred object, which impairs the detection of the object.

Secondly, a high frame rate is desired to follow the trajectory of a diffusing particle. In order to identify the same particle in two successive image frames, it is ideal to meet the Nyquist criterion in temporal sampling, that is, the displacement during the time interval should be less than half the spatial resolution. The previously measured diffusion coefficients of messenger ribonucleoprotein particles (mRNPs) in living cells are 0.1–0.8 $\mu m^2/s$ (Fusco *et al.*, 2003; Shav-Tal *et al.*, 2004), thus, the sampling time interval needs to be 5–40 ms. This requirement can be relaxed when the particle density in the image is sufficiently low. If the average distance between particles is much larger than the average particle displacement between frames, two successive images of an object can be linked to each other unambiguously. However, with increasing particle density, it becomes more difficult to solve the motion correspondence problem.

Lastly, a sufficient tracking range is crucial to identify the type of motion. The total number of frames in the image sequence determines the statistical accuracy of the analysis (Qian *et al.*, 1991; Saxton, 1997). Monte Carlo simulations can be performed without limitation on the tracking period to quantitatively estimate the deviations from Brownian motion. For instance, Saxton examined the statistical variation of the diffusion coefficient D by simulations (Saxton, 1997). In addition, longer observation enables the detection of motion-type transitions. Since it is difficult to meet all of these requirements with a limited number of photons, one needs to find a good compromise between the high acquisition rate and the total duration of the experiment.

4.2. Instrumentation

SPT may be performed in various forms of light microscopy, including wide-field, confocal, and total internal reflection microscopy (TIRFM). A standard wide-field epi-illumination microscope has been successfully used to visualize single mRNA molecules labeled by the MS2 system. The microscope system should be optimized to observe single molecule dynamics in living cells. For a sensitive detection of weak fluorescence, the photon collection efficiency needs to be maximized while the background noise is minimized.

Microscope objectives with higher NA are desirable to obtain a higher photon collection efficiency and tighter point-spread function. Large magnification may be beneficial to minimize the pixelation noise, as long as the particle under study does not travel beyond the field of view. When using multiple fluorophores with different emission colors, chromatic aberration must be appropriately corrected by using achromat or apochromat objectives. For colocalization of single molecules labeled with different fluorophores, multichannel image registration is also necessary (Churchman and Spudich, 2007).

The most common light source for wide-field microscopy is either a mercury or xenon arc lamp. If the power of the lamp at the excitation wavelength is not sufficient to detect single molecules, a laser light source can be employed. Laser illumination provides not only higher power but also narrower excitation bandwidth in the subnanometer range, which reduces the excitation background (Grunwald *et al.*, 2008b). Since the viability of the cell also needs to be ensured, the illumination power must be balanced to protect the specimen against photodamage and photobleaching.

For single-molecule detection, there are many different types of cameras and spot detectors. The most commonly used detector for SPT is the electron-multiplying charge-coupled device (EMCCD). The electron-multiplying shift register increases the gain while keeping the noise level low. In order to achieve shot noise-limited detection, it is desirable to obtain maximum quantum efficiency and minimum camera noise. For higher quantum efficiency, back-illuminated type CCD chips are preferable. The dark noise of the CCD is due to the thermal fluctuation in the amount of charge in total darkness and can be reduced by cooling the chip down to -80 °C. The readout noise increases approximately with the square root of the readout speed (Rasnik *et al.*, 2007). Therefore, there is a tradeoff between the acquisition rate and the noise level. A frame-transfer feature alleviates this constraint and is highly desirable for sufficiently frequent acquisition.

Finally, cells must be kept in physiological conditions to ensure that the dynamics observed is an appropriate representation of the behavior *in vivo*. For mammalian cells, the temperature should be maintained at 37 °C.

There are several commercial systems to keep the sample warm during imaging sessions. A simple economical method is to use heating elements for the specimen and the objective lens. However, there can be a thermal drift due to the cycles of heating and cooling. A more reliable method is to build an incubator around the microscope body. A custom-designed incubator that can enclose the majority part of the microscope can keep the system at a stable temperature and prevent thermal drift. Also, incubators are desirable to control the CO_2 level and humidity for extended periods of time.

4.3. 3D tracking

SPT has been mainly employed in two-dimensional systems such as cell surface or immobilized cytoskeletons *in vitro*. It is highly desirable to extend the technology into three-dimensional imaging since most biological processes occur within the 3D space of the cell. Kao and Verkman (1994) introduced a weak cylindrical lens in the detection optics of an epifluorescence microscope, which caused astigmatism in a particle image. Images of fluorescent beads are circular in the focus but become ellipsoidal when out of the focus. The major axis of the ellipsoid is rotated by 90° above and below the focus. They retrieved the x, y, and z positions by analyzing the shape, orientation, and position of the particle's image.

Simple defocusing methods have also been used for 3D tracking. Speidel *et al.* (2003) calibrated the radii of the ring patterns in the defocused image of a particle as a function of the axial position of the object. They found a linear dependence of the ring radii on the z-offset within an axial range of $\sim 3\ \mu$m. Toprak *et al.* (2007) employed a similar method but with simultaneous imaging of the focused and defocused planes, and improved the localization accuracy in 3D. 3D tracking is also demonstrated using a two-photon microscope by tracing the laser beam in four circular orbits surrounding the object (Levi *et al.*, 2005). The position of the particle is calculated on the fly, and those coordinates are used to set the next scanning position.

5. Analyzing mRNA Motions

A number of ideas and techniques for tracking objects in a sequence of images can be found in the context of fluid mechanics, computer vision, and radar surveillance. In cell biological applications, two types of tracking algorithms have typically been used. The first category detects the changes in particle positions by crosscorrelating consecutive frames. The second category generally consists of two steps: find the center of each particle in time-lapse images, and connect the positions to reconstruct the trajectory. Cheezum *et al.* (2001) compared the tracking algorithms quantitatively by

simulations. They concluded that the crosscorrelation method performs better for particles larger than the wavelength. Conversely, for particles that are smaller than the emission wavelength, it is more accurate and precise to perform particle detection followed by trajectory linking. Since the size of the mRNPs is smaller than the visible light wavelength, we will consider the second category of the tracking method here.

5.1. Localization algorithms

In light microscopy, an object that is smaller than the dimension of wavelength appears as a diffraction-limited spot. Because of the limited resolution, the details of the object cannot be discerned. However, the center of the object can be determined with a much better precision when a sufficient number of photons are collected from the particle. There are two major categories of algorithms to identify the location of single particles: searching for the intensity-weighted center of mass (centroid) or fitting image intensities by point-spread function.

In a centroid method, the image is filtered to remove high-frequency noise, a binary mask is applied to exclude the background below threshold intensity, and the weighted center of mass of contiguous pixels is calculated (Ghosh and Webb, 1994). Gelles *et al.* (1988) demonstrated a localization precision of 1–2 nm by usingDIC images of plastic beads. They cross-correlated the sequence of images with a kernel segment of a single bead image and computed the centroid of each particle. The centroid method is computationally efficient and valid for asymmetric particles. However, the precision and accuracy of the particle position found by centroid methods are highly dependent on the background threshold level (Cheezum *et al.*, 2001).

Alternatively, the fluorescent intensity distribution of a single particle can be fit with a 2D Gaussian function. It provides a higher localization precision and an accurate measure of the intensity (Anderson *et al.*, 1992). Cheezum *et al.* (2001) compared the efficacy of the centroid and Gaussian fitting routines and concluded that a direct Gaussian fit to the intensity profile is superior in terms of both accuracy and precision.

Thompson *et al.* (2002) derived an approximate equation for the localization precision:

$$\langle(\Delta x)^2\rangle = \frac{s^2 + a^2/12}{N} + \frac{8\pi s^4 b^2}{a^2 N^2} \tag{18.1}$$

where s is the standard deviation of the point-spread function, a is the pixel size, b is the background noise, and N is the photon number. In the shot noise limit (the first term in Eq. (18.1)), the localization error is inversely

proportional to the square root of the number of photons. When the background noise dominates (the second term in Eq. (18.1)), the uncertainty scales as the inverse of the number of photons. They also introduced a simplified fitting algorithm called ''Gaussian mask,'' which is equivalent to a nonlinear least-squares fit to a Gaussian distribution ignoring the shot noise. In this method, the centroid is calculated in convolution with a Gaussian distribution around the candidate position, and iterated until the centroid position converges. When the number of photons originating from the molecule of interest is small, the Gaussian mask algorithm can be more robust than the full least-squares fit.

5.2. Tracking algorithms

After the particles are located in a sequence of frames, the next step is to link a position in each frame with a corresponding position in the next frame. In general, the particles are not distinguishable from one another. With increasing particle density, it becomes more difficult to determine the next position of a given particle. Therefore, an important parameter to gauge the difficulty of particle tracking is the spacing-displacement ratio, which is the average distance between particles divided by the average particle displacement between two successive frames (Malik *et al.*, 1993). If the spacing-displacement ratio is much larger than one, tracking can be reliably done by simple nearest-neighbor approaches (Anderson *et al.*, 1992; Ghosh and Webb, 1994).

However, it becomes more difficult to connect the trajectories as the spacing-displacement ratio becomes smaller. Because there are many possible pairs of particles between two images, it is necessary to find the most probable set of connection. Various algorithms have been developed to seek a unique solution to the motion correspondence problem, and they can be divided into two broad categories: *deterministic* and *statistical* methods (Yilmaz *et al.*, 2006).

Deterministic methods are also called combinatorial optimization techniques. They define a cost function of associating each spot in the previous frame to a single spot in the next frame. By minimizing the cost function, an optimal assignment can be obtained. For example, Crocker and Grier (1996) described a simple cost function to track noninteracting Brownian particles. If we consider an ensemble of indistinguishable noninteracting M particles, the most probable set of linkages between two frames is obtained when $\sum_{j=1}^{M}(\overrightarrow{r_j}(i+1) - \overrightarrow{r_j}(i))^2$ is minimized. If the particles can be distinguished by additional information such as size, color, and intensity, these data can be treated as another dimension of the particles in the cost function. The algorithm is available at http://www.physics.emory.edu/~weeks/idl.

If the scope of the tracking is extended to more than two image frames, it becomes a multidimensional optimal assignment problem (Sbalzarini and Koumoutsakos, 2005; for the associated ImageJ plugin, see http://www.mosaic.ethz.ch/Downloads/ParticleTracker). Most multiframe tracking algorithms are based on heuristic assumptions such as smoothness of the particle trajectories motion (Sage *et al.*, 2005; for the associated ImageJ plugin, see http://bigwww.epfl.ch/sage/soft/spottracker/; Vallotton *et al.*, 2003). By tracking objects across multiple frames, the history of the particle movement is considered. Therefore, these methods can resolve problems arising from crossing trajectories, temporary occlusion, blinking, and detection failure. However, multiframe tracking is computationally expensive and becomes difficult to solve as the frame number increases. Therefore, greedy search techniques and heuristic approaches are used to obtain approximate solutions (reviewed in Jähne *et al.*, 2007; Yilmaz *et al.*, 2006).

Statistical data association methods take the uncertainty of the position measurements into account and assign a probability density function for a particle state. The probability distribution propagates over time and is updated by the measurements in each frame. The simplest statistical tracking method is the *Kalman filter*. In a Kalman filter, the initial particle state and noise have a Gaussian distribution. The next position of a particle is predicted by a linear model of motion, and the actual observation in the predicted search region is used to adjust the particle state. Kalman filtering can also be extended to multiple frame processing. The multiple hypotheses tracking (MHT) algorithm defers the correspondence decision until several frames are examined (Reid, 1979). Probabilities for multiple hypotheses are calculated, and the most likely set of track is chosen. The MHT algorithm seeks the globally optimal solution by considering all particle positions at all time frames. However, it is computationally intense both in time and memory. Thus, various approximate solutions to MHT were developed and applied to SPT in living cells (Jaqaman *et al.*, 2008; Serge *et al.*, 2008).

5.3. Categories of single particle motion

It is not known whether molecular motion in biology is finite, but the effort to categorize it is well worthwhile for SPT. Random walk is one of a few simple and universal models in physics, which analytically describes unobstructed, or ''normal,'' diffusion. Therefore, it is natural in SPT that normal diffusion serves as a reference while complicated motions are treated as deviations from this null model. A molecule may exhibit one of the five modes of motion, depending on the nature of interactions; stationary, normal diffusion, anomalous subdiffusion, corralled diffusion, and directional movement by active transport. Moreover, it is also possible that an

mRNA molecule makes transitions between the modes (Fusco *et al.*, 2003). It was only after SPT was applied that researchers began to recognize the significance of nonBrownian microscopic motions in biology (Feder *et al.*, 1996; Kusumi *et al.*, 1993).

A measurable parameter most commonly employed in SPT analysis is the mean-squared displacement (MSD) as a function of time. If we consider a trajectory $\overrightarrow{r}(t)$ recorded every δt for N time steps, the MSD for a given time lag $n\delta t$ is calculated by:

$$\langle r^2(n)\rangle = \frac{1}{N-n}\sum_{i=1}^{N-n}[\overrightarrow{r}(i+n) - \overrightarrow{r}(i)]^2$$

The MSD curves for the different types of motion are shown in Fig. 18.1 and the analytical forms can be expressed as follows:

$\langle r^2\rangle < (\Delta x)^2$	stationary (Δx: localization precision)
$\langle r^2\rangle = 2dDt$	normal diffusion (d: spatial dimension)
$\langle r^2\rangle = \Gamma t^{\alpha}$	anomalous subdiffusion ($\alpha < 1$)
$\langle r^2\rangle = R^2\left(1 - A_1 \exp\left(-\frac{A_2 t}{R^2}\right)\right)$	corralled diffusion (R: radius of the corral)
$\langle r^2\rangle = 2dDt + v^2t^2$	directed motion with diffusion (v: speed)

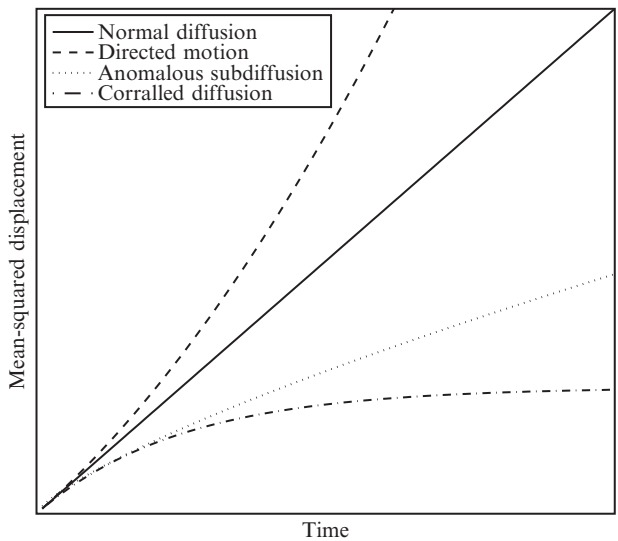

Figure 18.1 **Mean-squared displacement as a function of time for various modes of motion.**

When fitting experimental MSD data with these analytical functions, one needs to add a constant to the fit-function because the localization precision Δx leads to an offset in the MSD plot (Wieser and Schutz, 2008).

Another approach to analyze SPT trajectories is obtained by looking at the statistics of displacements, rather than the average. The probability distribution (Anderson *et al.*, 1992), or equivalently, the jump-distance distribution (Grunwald *et al.*, 2008a; Siebrasse *et al.*, 2008), permits different perspectives from MSD. While ensemble MSD analysis measures an average of a population, jump-distance histogram detects different mobility populations. Jump distance analysis measures the probability P to find a particle recorded within a distance of $\overrightarrow{r}(i+1)$ from the initial position $\overrightarrow{r}(t)$ after time t according to the following equation:

$$P(\overrightarrow{r}(i+1)|\overrightarrow{r}(i),t)\mathrm{d}V = \frac{1}{(4\pi Dt)^{d/2}} \exp\left(-\frac{(\overrightarrow{r}(i+1)-\overrightarrow{r}(i))^2}{4Dt}\right)\mathrm{d}V,$$

normal diffusion

The probability distribution is suited to distinguish subpopulations with multiple diffusion coefficients, which can be nontrivial to identify in MSD plots.

5.4. Interpretation of mRNA tracking data

Upon successful labeling, imaging, and tracking of mRNAs, SPT data provide a rich source of information. Linking the quantitative analysis of mRNA movement to a biological process or function is another big challenge. SPT often yields observational information about the nature of mRNA movement. Observational reports about the travels of mRNA in the nucleus have utilized mean-squared displacement (Politz *et al.*, 2006; Shav-Tal *et al.*, 2004) as well as jump-distance histograms (Grunwald *et al.*, 2008a; Siebrasse *et al.*, 2008) to describe the nuclear environment that the mRNA encounters. In these reports, MSD measurements yielded an average diffusion coefficient, while mean jump distance was used to calculate the mean diffusion coefficient of discernable populations in unique compartments.

While nuclear SPT of mRNA usually yields diffusion coefficients of mRNA in the various nuclear compartments or the entire nucleus, utilization of SPT of mRNA in the cytoplasm needs to distinguish between diffusing mRNAs and ones that are transported along cytoskeletal elements. The use of MSD to analyze SPT data is capable of comparing the distribution of distinct motility populations of mRNA in the cytoplasm of cells. For example, MSD has been used to compare the relative population of

diffusing mRNAs compared to transported or static mRNAs of reporter constructs with and without the β-actin 3′UTR (Fusco *et al.*, 2003).

Alternatively, a specific aspect of active transport may be measured, such as the average velocity, maximum velocity, or the average length of transport path. Rook *et al.* (2000) measured a variety of aspects of active transport of CamKII alpha mRNA in the neuronal dendrites pre- and post-potassium chloride (KCl) stimulation. They measured the percent motile mRNA granules, distance traveled, average rate, and the maximum rate of active transport. The comparison of the motility of mRNA prior and following a treatment or knockdown of RNA-binding proteins is a direct way to measure cellular elements responsible for mRNA localization or means in which mRNA localization can be induced. In this study, it was shown that following KCl stimulation, there was a shift of movement from oscillatory to anterograde. In a more recent study of CamKII mRNA in dendrites, MSD was used to compare the relative abundance of actively transported and nonmotile mRNAs in wild type and FMRP knockout neurons. SPT of mRNA also allowed the measurement of the maximal and mean granule velocity in both the anterograde and retrograde directions in dendrites (Dictenberg *et al.*, 2008). The measurement of mRNA velocity along the cytoskeleton is an important stepping stone toward understanding more about the nature of active transport in different cell types and situations. Because cytoskeletal filaments are required for active transport, studying the contribution of cytoskeletal elements and molecular motors on mRNA localization is often accomplished by chemical disruption of the cytoskeleton or overexpression of the dominant negative motors (Mingle *et al.*, 2005; Sundell and Singer, 1991; Zhang *et al.*, 1999). Conversely, live measurements of mRNA being actively transported can provide an insight into how cells actively facilitate the localization of mRNA to discrete locations.

6. Conclusions

SPT is a useful tool for monitoring the behavior of individual molecules in living cells, providing new information about dynamic heterogeneity. Current technological advances in SPT used in conjunction with the MS2-labeling system have allowed more accurate and extended tracking of mRNAs in cells. Single mRNA tracking studies are now elucidating the mechanisms of mRNA transport and localization in various cell types. Despite the remarkable recent progress, many important questions remain to be answered. A clear picture of the cause-and-effect relationship between mRNA localization and cell physiology will likely emerge as the *in vivo* dynamics of mRNA is revealed. Furthermore, multicolor imaging of single

mRNAs interacting with their diverse binding partners will provide a more comprehensive picture of the molecular pathways in live cells.

ACKNOWLEDGMENTS

This work was supported by National Institutes of Health grant EB2060. H. Y. P. was also supported by National Research Service Awards 5T32 HL007675 and 1F32 GM087122.

REFERENCES

Ainger, K., *et al.* (1993). Transport and localization of exogenous myelin basic protein mRNA microinjected into oligodendrocytes. *J. Cell. Biol.* **123,** 431–441.

Anderson, C. M., *et al.* (1992). Tracking of cell surface receptors by fluorescence digital imaging microscopy using a charge-coupled device camera. Low-density lipoprotein and influenza virus receptor mobility at 4 degrees C. *J. Cell. Sci.* **101**(Pt 2), 415–425.

Axelrod, D., *et al.* (1976). Mobility measurement by analysis of fluorescence photobleaching recovery kinetics. *Biophys. J.* **16,** 1055–1069.

Barak, L. S., and Webb, W. W. (1982). Diffusion of low density lipoprotein–receptor complex on human fibroblasts. *J. Cell. Biol.* **95,** 846–852.

Beach, D. L., *et al.* (1999). Localization and anchoring of mRNA in budding yeast. *Curr. Biol.* **9,** 569–578.

Bertrand, E., *et al.* (1998). Localization of ASH1 mRNA particles in living yeast. *Mol. Cell.* **2,** 437–445.

Bobroff, N. (1986). Position measurement with a resolution and noise-limited instrument. *Rev. Sci. Instrum.* **57,** 1152.

Bratu, D. P., *et al.* (2003). Visualizing the distribution and transport of mRNAs in living cells. *Proc. Natl. Acad. Sci. USA* **100,** 13308–13313.

Chao, J. A., *et al.* (2008a). Using the bacteriophage MS2 coat protein-RNA binding interaction to visualise RNA in living cells. *In* "Probes and Tags to Study Biomolecular Function," (L. W. Miller, ed.), Wiley-VCH, Weinheim.

Chao, J. A., *et al.* (2008b). Structural basis for the coevolution of a viral RNA–protein complex. *Nat. Struct. Mol. Biol.* **15,** 103–105.

Cheezum, M. K., *et al.* (2001). Quantitative comparison of algorithms for tracking single fluorescent particles. *Biophys. J.* **81,** 2378–2388.

Churchman, L. S., and Spudich, J. A. (2007). Colocalization of fluorescent probes: Accurate and precise registration with nanometer resolution. *In* "Single-Molecule Techniques: A Laboratory Manual," (P. Selvin and T. Ha, eds.), pp. 73–84. Cold Spring Harbor Laboratory Press, Cold Spring Harbor.

Condeelis, J., and Singer, R. H. (2005). How and why does beta-actin mRNA target? *Biol. Cell* **97,** 97–110.

Crocker, J. C., and Grier, D. G. (1996). Methods of digital video microscopy for colloidal studies. *J. Colloid Interface Sci.* **179,** 298–310.

De Brabander, M., *et al.* (1985). Probing microtubule-dependent intracellular motility with nanometer particle video ultramicroscopy (nanovid ultramicroscopy). *Cytobios* **43,** 273–283.

Dictenberg, J. B., *et al.* (2008). A direct role for FMRP in activity-dependent dendritic mRNA transport links filopodial-spine morphogenesis to fragile X syndrome. *Dev. Cell* **14,** 926–939.

Edidin, M., *et al.* (1991). Lateral movements of membrane-glycoproteins restricted by dynamic cytoplasmic barriers. *Science* **254,** 1379–1382.
Eggeling, C., *et al.* (2005). Molecular photobleaching kinetics of Rhodamine 6G by one- and two-photon induced confocal fluorescence microscopy. *Chemphyschem* **6,** 791–804.
Einstein, A. (1905). Investigations on the Theory of the Brownian Movement. Dover Publications, Inc., New York.
Farina, K. L., and Singer, R. H. (2002). The nuclear connection in RNA transport and localization. *Trends Cell Biol.* **12,** 466–472.
Feder, T. J., *et al.* (1996). Constrained diffusion or immobile fraction on cell surfaces: A new interpretation. *Biophys. J.* **70,** 2767–2773.
Fusco, D., *et al.* (2003). Single mRNA molecules demonstrate probabilistic movement in living mammalian cells. *Curr. Biol.* **13,** 161–167.
Gelles, J., *et al.* (1988). Tracking kinesin-driven movements with nanometre-scale precision. *Nature* **331,** 450–453.
Ghosh, R. N., and Webb, W. W. (1994). Automated detection and tracking of individual and clustered cell-surface low-density-lipoprotein receptor molecules. *Biophys. J.* **66,** 1301–1318.
Grunwald, D., *et al.* (2008a). Probing intranuclear environments at the single-molecule level. *Biophys. J.* **94,** 2847–2858.
Grunwald, D., *et al.* (2008b). Cell biology of mRNA decay. *Methods Enzymol.* **448,** 553–577.
Ishihama, Y., and Funatsu, T. (2009). Single molecule tracking of quantum dot-labeled mRNAs in a cell nucleus. *Biochem. Biophys.l Res. Commun.* **381,** 33–38.
Jähne, B., *et al.* (2007). Data analysis. *In* ''Springer Handbook of Experimental Fluid Mechanics,'' (C. Tropea, *et al.*, eds.), pp. 1474–1481. Springer, Berlin/Heidelberg.
Jaqaman, K., *et al.* (2008). Robust single-particle tracking in live-cell time-lapse sequences. *Nat. Methods* **5,** 695–702.
Kao, H. P., and Verkman, A. S. (1994). Tracking of single fluorescent particles in three dimensions: Use of cylindrical optics to encode particle position. *Biophys. J.* **67,** 1291–1300.
Knowles, R. B., *et al.* (1996). Translocation of RNA granules in living neurons. *J. Neurosci.* **16,** 7812–7820.
Kusumi, A., *et al.* (1993). Confined lateral diffusion of membrane-receptors as studied by single-particle tracking (nanovid microscopy)—Effects of calcium-induced differentiation in cultured epithelial-cells. *Biophys. J.* **65,** 2021–2040.
Kusumi, A., *et al.* (1998). Application of laser tweezers to studies of the fences and tethers of the membrane skeleton that regulate the movements of plasma membrane proteins. *Methods Cell Biol.* **55,** 173–194.
Kusumi, A., *et al.* (2005). Paradigm shift of the plasma membrane concept from the two-dimensional continuum fluid to the partitioned fluid: High-speed single-molecule tracking of membrane molecules. *Ann. Rev. Biophys. Biomol. Struct.* **34,** 351–378.
Lawrence, J. B., and Singer, R. H. (1986). Intracellular-localization of messenger-rnas for cytoskeletal proteins. *Cell* **45,** 407–415.
Levi, V., and Gratton, E. (2007). Exploring dynamics in living cells by tracking single particles. *Cell Biochem. Biophys.* **48,** 1–15.
Levi, V., *et al.* (2005). 3-D particle tracking in a two-photon microscope: Application to the study of molecular dynamics in cells. *Biophys. J.* **88,** 2919–2928.
Malik, N. A., *et al.* (1993). Particle tracking velocimetry in 3-dimensional flows. 2. Particle tracking. *Exp. Fluids* **15,** 279–294.
Martin, K. C., and Ephrussi, A. (2009). mRNA localization: Gene expression in the spatial dimension. *Cell* **136,** 719–730.

Mingle, L. A., *et al.* (2005). Localization of all seven messenger RNAs for the actin-polymerization nucleator Arp2/3 complex in the protrusions of fibroblasts. *J. Cell Sci.* **118,** 2425–2433.
Nirmal, M., *et al.* (1996). Fluorescence intermittency in single cadmium selenide nanocrystals. *Nature* **383,** 802–804.
Pederson, T. (2001). Fluorescent RNA cytochemistry: Tracking gene transcripts in living cells. *Nucleic Acids Res.* **29,** 1013–1016.
Perrin, J. (1913). Atoms. D. Van Nostrand Company, New York.
Politz, J. C. R., *et al.* (2006). Rapid, diffusional shuttling of Poly(A) RNA between nuclear speckles and the nucleoplasm. *Mol. Biol. Cell* **17,** 1239–1249.
Qian, H., *et al.* (1991). Single particle tracking. Analysis of diffusion and flow in two-dimensional systems. *Biophys. J.* **60,** 910–921.
Querido, E., and Chartrand, P. (2008). Using fluorescent proteins to study mRNA trafficking in living cells. *In* ''Fluorescent Proteins,'' 2nd ed., Vol. 85, 273 pp. Elsevier Academic Press Inc., San Diego.
Rasnik, I., *et al.* (2006). Nonblinking and long-lasting single-molecule fluorescence imaging. *Nat. Methods* **3,** 891–893.
Rasnik, I., *et al.* (2007). Electronic cameras for low-light microscopy. *In* ''Digital Microscopy,'' (G. Sluder and D. E. Wolf, eds.), p. 228. Elsevier Academic Press, Amsterdam.
Reid, D. B. (1979). An algorithm for tracking multiple targets. *IEEE Trans. Autom. Control* AC-24.
Rodriguez, A. J., *et al.* (2007). Imaging mRNA movement from transcription sites to translation sites. *Semin. Cell Dev. Biol.* **18,** 202–208.
Rook, M. S., *et al.* (2000). CaMKII alpha 3′ untranslated region-directed mRNA translocation in living neurons: Visualization by GFP linkage. *J. Neurosci.* **20,** 6385–6393.
Sage, D., *et al.* (2005). Automatic tracking of individual fluorescence particles: Application to the study of chromosome dynamics. *IEEE Trans. Image Process.* **14,** 1372–1383.
Santangelo, P. J., *et al.* (2009). Single molecule-sensitive probes for imaging RNA in live cells. *Nat. Methods* **6,** 347–349.
Saxton, M. J. (1997). Single-particle tracking: The distribution of diffusion coefficients. *Biophys. J.* **72,** 1744–1753.
Saxton, M. J., and Jacobson, K. (1997). Single-particle tracking: Applications to membrane dynamics. *Ann. Rev. Biophys. Biomol. Struct.* **26,** 373–399.
Sbalzarini, I. F., and Koumoutsakos, P. (2005). Feature point tracking and trajectory analysis for video imaging in cell biology. *J. Struct. Biol.* **151,** 182–195.
Serge, A., *et al.* (2008). Dynamic multiple-target tracing to probe spatiotemporal cartography of cell membranes. *Nat. Methods* **5,** 687–694.
Shan, J. G., *et al.* (2003). A molecular mechanism for mRNA trafficking in neuronal dendrites. *J. Neurosci.* **23,** 8859–8866.
Shav-Tal, Y., and Singer, R. H. (2005). RNA localization. *J. Cell Sci.* **118,** 4077–4081.
Shav-Tal, Y., *et al.* (2004). Dynamics of single mRNPs in nuclei of living cells. *Science* **304,** 1797–1800.
Sheetz, M. P., *et al.* (1989). Nanometre-level analysis demonstrates that lipid flow does not drive membrane glycoprotein movements. *Nature* **340,** 284–288.
Siebrasse, J. P., *et al.* (2008). Discontinuous movement of mRNP particles in nucleoplasmic regions devoid of chromatin. *Proc. Natl. Acad. Sci. USA* **105,** 20291–20296.
Smith, A. M., *et al.* (2008). Bioconjugated quantum dots for in vivo molecular and cellular imaging. *Advan. Drug Deliv. Rev.* **60,** 1226–1240.
Speidel, M., *et al.* (2003). Three-dimensional tracking of fluorescent nanoparticles with subnanometer precision by use of off-focus imaging. *Opt. Lett.* **28,** 69–71.
Sundell, C. L., and Singer, R. H. (1991). Requirement of microfilaments in sorting of actin messenger-RNA. *Science* **253,** 1275–1277.

Thompson, R. E., *et al.* (2002). Precise nanometer localization analysis for individual fluorescent probes. *Biophys. J.* **82,** 2775–2783.
Toprak, E., *et al.* (2007). Three-dimensional particle tracking via bifocal imaging. *Nano Lett.* **7,** 2043–2045.
Tyagi, S. (2009). Imaging intracellular RNA distribution and dynamics in living cells. *Nat. Methods* **6,** 331–338.
Vallotton, P., *et al.* (2003). Recovery, visualization, and analysis of actin and tubulin polymer flow in live cells: A fluorescent speckle microscopy study. *Biophys. J.* **85,** 1289–1306.
Widengren, J., *et al.* (2007). Strategies to improve photostabilities in ultrasensitive fluorescence spectroscopy. *J. Phys. Chem. A.* **111,** 429–440.
Wieser, S., and Schutz, G. J. (2008). Tracking single molecules in the live cell plasma membrane—Do's and Don't's. *Methods* **46,** 131–140.
Yamagishi, M., *et al.* (2009). Single-molecule imaging of beta-actin mRNAs in the cytoplasm of a living cell. *Exp. Cell Res.* **315,** 1142–1147.
Yilmaz, A., *et al.* (2006). Object tracking: A survey. *ACM Comput. Surv.* **38,** 1–45.
Zhang, H. L., *et al.* (1999). Neurotrophin regulation of beta-actin mRNA and protein localization within growth cones. *J. Cell Biol.* **147,** 59–70.
Zimyanin, V. L., *et al.* (2008). In vivo Imaging of oskar mRNA transport reveals the mechanism of posterior localization. *Cell* **134,** 843–853.